

# FIRST XMM-NEWTON RESULTS ON THE PULSAR WIND NEBULA IN THE COMPOSITE SUPERNOVA REMNANT G0.9+0.1

D. Porquet<sup>1</sup>, A. Decourchelle<sup>1</sup>, and R.S. Warwick<sup>2</sup>

<sup>1</sup>Service d'Astrophysique, CEA Saclay, 91191 Gif-sur-Yvette Cedex, France

<sup>2</sup>Department of Physics and Astronomy, University of Leicester, Leicester LE1 7RH, UK

## ABSTRACT

We report the results of the *XMM-Newton* observation of the Pulsar Wind Nebula (PWN) in the composite supernova remnant G0.9+0.1 located in the Galactic Center region. Thanks to the sensitivity of the EPIC cameras, we focus on the first spectral analysis of large and small-scale structures of this PWN using MOS and PN data in combination. Our spatially resolved spectral analysis at large-scale offers a clear indication of a softening of the photon index with distance from the centroid of the nebula (from  $\Gamma_{\text{core}}=1.12^{+0.45}_{-0.48}$  to  $\Gamma=2.42^{+0.19}_{-0.19}$ ), as observed in other known X-ray plerions. A spectral analysis of the small-scale structures in the central region of this PWN, delineates variations of the spectral index within the arc-like feature observed with *Chandra*: the eastern part has a hard photon index ( $\Gamma \sim 1.2 \pm 0.5$ ), while the south-west part has a softer photon index ( $\Gamma \sim 2.8 \pm 0.7$ ).

Key words: ISM: supernova remnants: individual: G0.9+0.1  
– X-rays: ISM

## 1. INTRODUCTION

G0.9+0.1 is the only composite SNR known in the direction of the GC ( $d \sim 10$  kpc,  $\mathcal{N}_H \sim 10^{23} \text{ cm}^{-2}$ ): a bright centrally condensed synchrotron nebula (with relatively flat spectral index), powered by the loss of rotational energy from the neutron star, and a radio shell with a steeper radio spectrum (Helfand & Becker 1987). Sidoli et al. (2000) were able to fit the *BeppoSAX* X-ray spectrum of the PWN with a power-law and interpret the X-ray emission as non-thermal in origin. The small angular extent of the X-ray emission (radius  $\sim 1'$ ), combined with an estimated age of the remnant of a few thousand years, is further evidence that the central radio core is powered by a young pulsar ( $\sim 2,700$  yr; Sidoli et al. 2000). Recently, G0.9+0.1 was observed with *Chandra* by Gaensler et al. (2001). They found that the synchrotron-emitting pulsar wind nebula (PWN) has a clear axial symmetry and a faint X-ray point source lying along the symmetry axis possibly corresponds to the pulsar itself. They argued that the nebular morphology can be explained in terms of a torus of emission in the pulsar's equatorial plane and a jet directed

along the pulsar spin axis, as is seen in the X-ray nebulae powered by other young pulsars (Crab, Vela). Here, we present the observations of G0.9+0.1 obtained with *XMM-Newton* and we focus on the first spectral analysis of the large and small-scale structures of the PWN (for more details see Porquet, Decourchelle & Warwick 2002).

## 2. OBSERVATIONS AND DATA ANALYSIS

We present in this section the spectral analysis of the PWN using combined fits of the MOS and PN data. The observation time after screening rejection of the flares are respectively for MOS1 and MOS2 about 15.5 ksec and 15.4 ksec, and 10 ksec for PN. We use the following camera response matrices: m1\_medv9q20t5r6\_all\_15.rsp, m2\_medv9q20t5r6\_all\_15.rsp, epn\_ef20\_sdY9\_medium.rsp. The local background used corresponds to the central MOS 1 CCD region excluding the bright point sources and the central part within a radius of 2.6'. We subtract from the source and the local background in our pointing, a blank-field observation (kindly provided by David Lumb) at the same position in order to take into account the particle background (see e.g. Majerowicz & Neumann 2001). The normalization between our pointing and the blank-field files is determined respectively by the count rate ratio in the 10–12 keV range for the MOS and 12–14 keV for the PN. The EPIC spectra were binned to give  $S/N \geq 3$ . XSPEC v11.1.0 was used for the spectral analysis. All subsequent errors are quoted at 90% confidence. Abundances are those of Anders & Grevesse (1989).

## 3. THE OVERALL NEBULA

The *XMM-Newton* observation of the supernova remnant G0.9+0.1 shows emission from the PWN, but not from the surrounding shell observed in radio. The soft X-ray emission expected from the shell is likely not seen due to the large interstellar absorption towards the source. The EPIC image of the PWN in G0.9+0.1 is presented in Figure 1. It exhibits a very bright central core, surrounded by extended diffuse emission. The extent of this emission is about twice larger than observed with *Chandra*, thanks to the high sensitivity of *XMM-Newton*.

For comparison with previous analysis, we fit the spectrum of the overall nebula. The region considered corresponds to the sum of the core with regions 1, 2 and 3, as

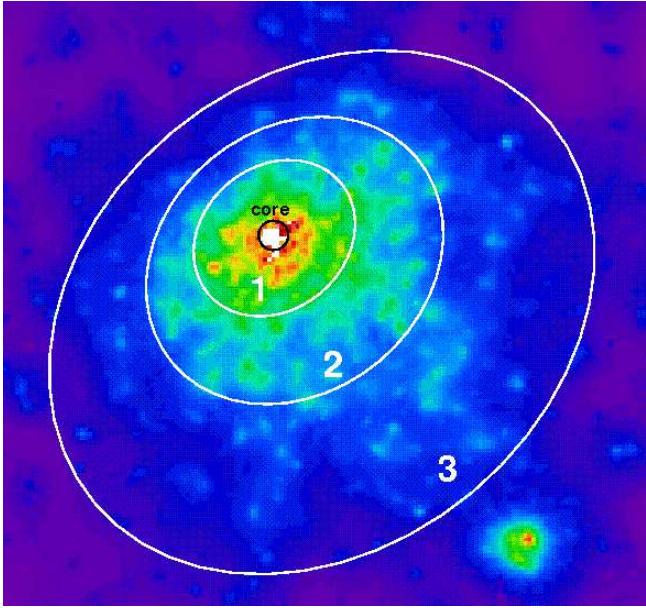


Figure 1. XMM-Newton (EPIC) image in the 3-8 keV energy band of the PWN in G0.9+0.1 obtained with an adaptive smoothing of signal to noise of 5. This size of the image is  $2.7' \times 2.7'$ . The different large-scale regions used for the spectral analysis are superposed.

is shown in Figure 1. The data are well fitted by either a power-law or a thermal bremsstrahlung (Table 1). For the photo-electric absorption, we use the cross-sections of Morrison & McCammon (1983). The parameters ( $\mathcal{N}_H$ ,  $\Gamma$ ) related to the power-law are compatible, within the error bars, with the *BeppoSAX* values (Sidoli et al. 2000:  $\mathcal{N}_H = 10.9^{+2.4}_{-2.1} \text{ cm}^{-2}$ ,  $\Gamma = 1.95^{+0.33}_{-0.30}$ ), though slightly higher but more tightly constrained. In the following, we use the updated cross-sections for X-ray absorption by the ISM (TBABS in XSPEC) from Wilms et al. (2000). The parameters although in good agreement with the previous ones (see Table 1), give systematically slightly lower  $\mathcal{N}_H$  values using TBABS absorption model.

#### 4. THE LARGE-SCALE STRUCTURES

The XMM-Newton data enables us to study the variation of the spectral index within the PWN. In other plerions, a softening of the spectrum has been observed toward the outer regions like in 3C 58 (Torii et al. 2000, Bocchino et al. 2001), G21.5-0.9 (Slane et al. 2000, Warwick et al. 2001) and IC 443 (Bocchino & Bykov 2001). This softening could be explained by the shorter lifetime of high energy electrons than for the lower energy electrons.

To search for this effect, we extracted the spectra in four regions, which are displayed in Figure 1. The observed spectra and best-fit models for the regions 1 (top panel) and 3 (bottom panel) are shown, as examples, in Figure 2. The spectrum extends up to almost 12 keV for the PN

Table 1. Results of the spectral fits for the overall X-ray PWN (core and regions 1, 2, 3 in Fig. 1). Cross-sections of the interstellar absorption are from Morrison & McCammon (1983; WABS in XSPEC) or from Wilms et al. (2000; TBABS). Uncertainties are quoted at 90% confidence. The unabsorbed fluxes (2-10 keV) are expressed in  $10^{-12} \text{ erg cm}^{-2} \text{ s}^{-1}$ .

Model	$\mathcal{N}_H$ ( $10^{23} \text{ cm}^{-2}$ )	$\Gamma$ or $kT$ (keV)	$\chi^2$ (446 dof)	$F_{2-10}^{unabs}$
wabs*PL	$1.46^{+0.14}_{-0.13}$	$2.00^{+0.19}_{-0.18}$	376.4	5.74
wabs*brems	$1.33^{+0.11}_{-0.10}$	$10.6^{+4.1}_{-2.2}$	376.1	5.11
wabs*bb	$0.83^{+0.09}_{-0.08}$	$1.73^{+0.05}_{-0.08}$	389.0	3.63
tbabs*PL	$1.39^{+0.13}_{-0.13}$	$1.94^{+0.18}_{-0.18}$	375.2	5.69
tbabs*brems	$1.27^{+0.10}_{-0.10}$	$11.5^{+4.8}_{-2.6}$	375.0	5.12
tbabs*bb	$0.80^{+0.09}_{-0.08}$	$1.75^{+0.09}_{-0.08}$	387.9	3.65

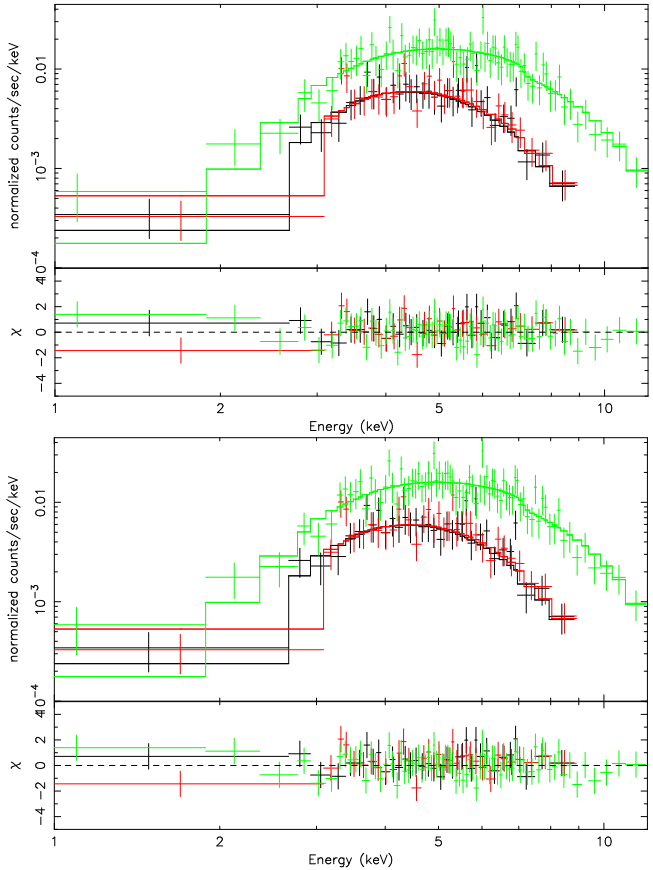


Figure 2. Spectral fits of the EPIC data (black for MOS 1, red for MOS2 and green for PN) with an absorbed power-law (TBABS\*PO). The inferred parameters are given in Table 2. Top panel: Region 1. Bottom panel: Region 3.

data, and to about 9 keV in the MOS data allowing strong constraints on the determination of the photon index.

We fit the spectra of these four regions by absorbed power-laws, fixing  $\mathcal{N}_H$  to the value obtained for the overall PWN, i.e.  $\mathcal{N}_H = 1.43 \cdot 10^{23} \text{ cm}^{-2}$  (see Table 1). The best-fit

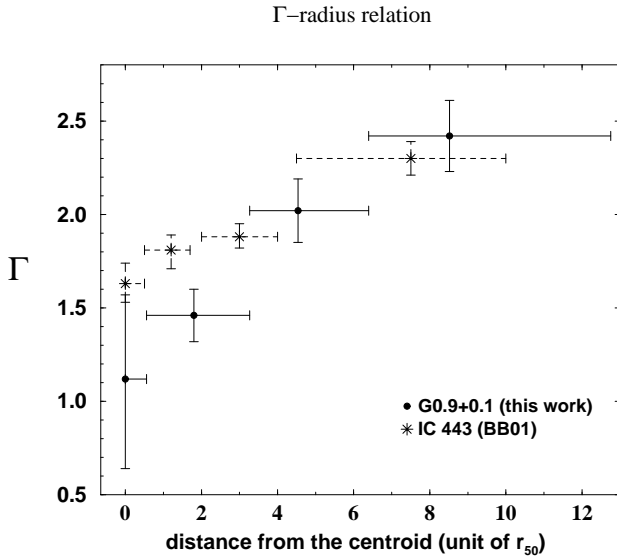


Figure 3. Variation of the spectral index versus distance to the centroid of the nebula. The X-axis shows the weighted mean distance of the pixels in a given region from the centroid expressed in unit of  $r_{50}$ , the radius at which the plerion surface brightness drops by a factor of 2 ( $7.15''$  for G0.9+0.1), as defined in Bocchino & Bykov (2001). For comparison, data for IC 443 are also plotted (taken from Bocchino & Bykov 2001).

parameters are given in Table 2. Letting the absorption column densities free do not afford significantly better fits, and the values of column density  $\mathcal{N}_H$  are compatible to within 15% for the different regions of the nebula.

A clear steepening of the spectrum is observed from the inner part toward the outer part of the PWN as is shown in Figure 3. The observed spectral softening with radius in G0.9+0.1 from the core to the outskirts of the PWN, is

Table 2. Combined fits of the regions of the PWN in G0.9+0.1. The cross-sections of the interstellar absorption are from Wilms et al. (2000). Unabsorbed X-ray flux (2-10 keV) are expressed in  $10^{-12}$  ergs  $\text{cm}^{-2} \text{s}^{-1}$ . Top:  $\mathcal{N}_H$  is frozen to the value obtained for the overall PWN (see Table 1). Bottom:  $\mathcal{N}_H$  is a free parameter.

	$\mathcal{N}_H^{(a)}$ ( $10^{23} \text{ cm}^{-2}$ )	$\Gamma$	$\chi^2/\text{dof}$	$F_X^{(b)}$ (2-10 keV)
core	1.39	$1.12^{+0.45}_{-0.48}$	15.8/18	0.25
region 1	1.39	$1.46^{+0.14}_{-0.14}$	103.4/146	1.79
region 2	1.39	$2.02^{+0.17}_{-0.17}$	121.6/136	1.65
region 3	1.39	$2.42^{+0.19}_{-0.19}$	161.8/173	2.02
core	$1.45^{+0.88}_{-0.66}$	$1.18^{+1.17}_{-0.99}$	15.8/17	0.26
region 1	$1.53^{+0.25}_{-0.22}$	$1.62^{+0.30}_{-0.28}$	102.3/145	1.93
region 2	$1.54^{+0.27}_{-0.23}$	$2.21^{+0.38}_{-0.34}$	120.6/135	1.83
region 3	$1.35^{+0.24}_{-0.21}$	$2.36^{+0.39}_{-0.36}$	161.7/172	1.95

most likely due to the effect of synchrotron radiation losses on the highest energy electrons as they progress through the nebula. For comparison we have reported on Figure 3 the variation of the spectral index inferred from the observation of IC 443 by Bocchino & Bykov (2001). The axis unit used ( $r_{50}$ , as defined in Fig. 3 and in Bocchino & Bykov 2001) gives a measure independent on the distance to the nebulae. Our data appear to show a stronger softening from the core to the outer part of the nebula of G0.9+0.1, compared to IC 443 (see Fig. 3), and also to other PWNe such as 3C 58 and G21.5-0.9 (see for comparison Fig. 5 in Bocchino & Bykov 2001). This could be consistent with a stronger magnetic field in the Galactic Center region compared to other SNR environments.

## 5. THE SMALL-SCALE STRUCTURES

The brightest region of the nebula corresponds to a core of angular diameter  $8''$  as observed with XMM-Newton. The Chandra observation has resolved it as an elliptical clump of size  $5'' \times 8''$  (Gaensler et al. 2001). The faint point source proposed to be the pulsar by Gaensler et al. (2001) is outside this region (about  $8''$  from the center

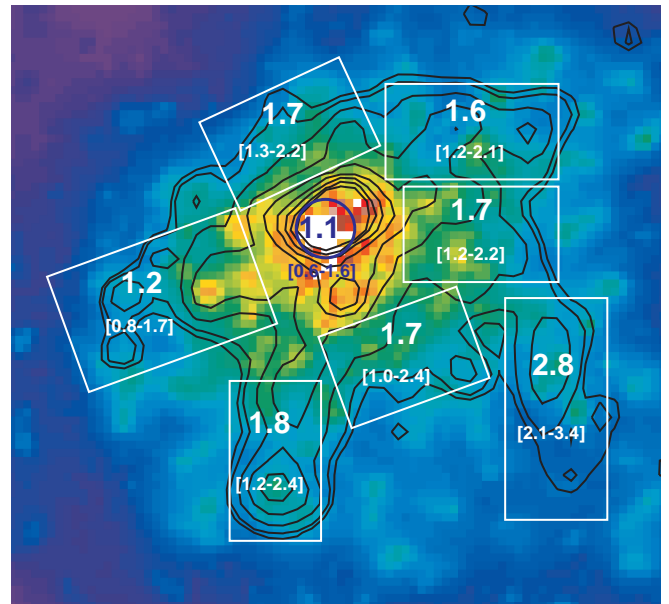


Figure 4. Close-up view with XMM-Newton (EPIC) of the center of the nebula in the 3-8 keV energy band obtained with an adaptative smoothing of signal to noise of 5. The size of the image is  $1.7' \times 1.3'$ . The contours (in black) corresponds to the Chandra observation in the same energy range. The white boxes represent different small-scale structures surrounding the bright core (dark blue circle), for which the spectral index and 90% confidence uncertainties are given. The position of the structures were determined according to the Chandra observation (see Gaensler et al. 2001): “East arc” ( $\Gamma \sim 1.2$ ), “jet” ( $\Gamma \sim 1.8$ ), and “South-West arc” ( $\Gamma \sim 2.8$ ).

of the clump). The fact that the hardest spectral index is obtained for the core would likely indicate that it hosts the pulsar. As proposed by Gaensler et al. (2001), this clump may also be an analog to the knots observed in the Crab nebula (Hester et al. 1995) and close to the Vela pulsar (Pavlov et al. 2001), which exhibit variability in brightness, position and morphology. The position and the morphology are however very similar in both *XMM-Newton* and *Chandra* observations which are separated from only about one month. The nature of the bright core is still unclear: a clump, which could be a region of separate particle acceleration as in PSR B1509-58 (Gaensler et al. 2002), or a very compact region in which the pulsar is embedded?.

Tracing the spectral variations in the small-scale structures around the core is then essential for understanding this particular PWN. Figure 4 displays a closer view of the inner region and shows the small-scale structures present around the core of PWN G0.9+0.1. For comparison, the X-ray contours of the *Chandra* data are superposed. In our data, the small-scale structures are not so clearly detected as with *Chandra* (jet-like and arc-like features). However using the position of the structures seen by *Chandra* and the high sensitivity of *XMM-Newton*, we were for the first time able to carry out spectral analysis of these small-scale structure. Determining their spectral index gives an indication of the geometry and orientation of the nebula. Figure 4 reports the photon spectral index of the corresponding structures obtained with combined fits (MOS and PN). The region corresponding to the eastern part of the arc-like feature in Gaensler et al. (2001), shows the hardest spectral index ( $\Gamma \sim 1.2 \pm 0.5$ ) among all the structures together with the core region ( $\Gamma \sim 1.1 \pm 0.5$ ). On the contrary the region corresponding to the south-west part of the arc-like feature, appears to have the steepest photon index ( $\Gamma \sim 2.8 \pm 0.7$ ) over all the PWN. A possible explanation is that the east arc is pointing towards the observer and that its spectral hardness is due to the relativistic beaming or Doppler boosting of the electrons, while the south-west arc is the opposite part of the torus. The region associated to the jet-like feature in Gaensler et al. (2001) does not exhibit a harder spectrum as suggested by their hardness ratio.

## 6. CONCLUSION

We report *XMM-Newton* observations of the X-ray Pulsar Wind Nebula (PWN) inside the composite supernova remnant G0.9+0.1 (Helfand & Becker 1987), which was convincingly detected for the first time in X-rays by *BepoSAX* (Mereghetti et al. 1998).

The large-scale image of the PWN G0.9+0.1 shows a very bright central core, surrounded by relatively large-scale diffuse emission with a much spatial extent than is apparent for the recent *Chandra* images. Thanks to its high sensitivity, *XMM-Newton* allows for the first time a

spectral analysis of the large and small-scale structures (see also Porquet, Decourchelle & Warwick 2002). Our spectral analysis combining the MOS and PN data offers a clear indication of a softening of the spectrum with distance from the centroid (related to the finite lifetime of the synchrotron emitting electrons), as observed in other known X-ray plerions. Even if in our data, the small-scale structures are not so clearly detected as in the *Chandra* data (jet-like and arc-like features), we were able for the first time to carry out their spectral analysis. Two of the structures show distinct spectral indexes from the general trend (from  $\Gamma \sim 1.6 \pm 0.5$  to  $\Gamma \sim 1.8 \pm 0.6$ ) : the eastern part of the arc-like feature has a very hard photon index ( $\Gamma \sim 1.2 \pm 0.5$ ), while the south-west part of the arc-like feature has a softer photon index ( $\Gamma \sim 2.8 \pm 0.7$ ).

The study of G0.9+0.1 provides further clues concerning the processes by which pulsars connect with their environment and also illustrates the impact of a strong ambient magnetic field as in the Galactic Center region.

## ACKNOWLEDGEMENTS

D.P. acknowledges grant support from the “Institut National des Sciences de l’Univers” and from the “Centre National d’Etudes Spatial” (France).

## REFERENCES

Anders E. & Grevesse N., 1989, *Geochimica et Cosmochimica Acta*, 53, 197  
 Bocchino F. & Bykov A. M., 2001, *A&A*, 376, 248  
 Bocchino F., Warwick, R. S., Marty, P., Lumb, D., Becker, W., Pigot, C. 2001, *A&A*, 369, 1078  
 Gaensler, B.M., Pivovaroff M.J., Garmire G.P. 2001, *ApJ*, 556, L107  
 Gaensler, B.M., Arons, J., Kaspi, V.M., Pivovaroff, M.J., Kawai, N., Tamura, K. 2002, *ApJ*, 569, in press  
 Helfand D.J. & Becker R.H., 1987, *ApJ* 314, 203  
 Hester J. J., Scowen P. A., Sankrit R., et al., 1995, *ApJ*, 448, 240  
 Majerowicz, S. & Neumann D. M. 2001, in the “XXI Moriond Conference”, Eds. D. Neumann, F. Durret, & J. Tran Thanh Van, in press ([http://www-dapnia.cea.fr/Conferences/Morion\\_astro\\_2001/index.html](http://www-dapnia.cea.fr/Conferences/Morion_astro_2001/index.html))  
 Mereghetti S., Sidoli L., Israel G. L. 1998, *A&A*, 331, L77  
 Morrison R. & McCammon D., 1983, *ApJ*, 270, 119  
 Pavlov, G. G., Kargaltsev, O. Y., Sanwal, D., Garmire, G. P. 2001, *ApJ*, 554, L189  
 Porquet, D., Decourchelle A., Warwick R.S., 2002, in preparation  
 Sidoli L., Mereghetti S., Israel G. L., Bocchino F., 2000, *A&A*, 361, 719  
 Slane P., Chen, Y., Schulz, N. S., Seward, F. D., Hughes, J. P., Gaensler, B. M. 2000, *ApJ*, 533, L29  
 Torii K., Slane, P. O., Kinugasa, K., Hashimoto, K., Tsunemi, H. 2000, *PASJ*, 52, 875  
 Warwick R. S., Bernard, J.-P., Bocchino, F., Decourchelle, A., Ferrando, P., Griffiths, R. G., Haberl, F., La Palombara, N., Lumb, D., Mereghetti, S., Read, A. M., Schaudel, D., Schurch, N., Tiengo, A., Willingale, R. 2001, *A&A*, 365, L248

Wilms J., Allen A., McCray R., 2000, ApJ, 542, 914